SUPPLEMENT TO THE *WELDING JOURNAL*, MAY 2012
Sponsored by the American Welding Society and the Welding Research Council

Reagent Selection in Austenitic Stainless Steel Solidification Modes Characterization

Out of eight different reagents tested to etch austenitic stainless steel weld metal, two showed the best results for microstructural characterization of solidification modes

BY M. ASUNCIÓN VALIENTE BERMEJO

ABSTRACT

Although a wide range of reagents is recommended for the microstructural characterization of stainless steels in the literature, the current research compares eight different reagents according to the following criteria: clear contrast between austenite and ferrite phases and morphologies, etching temperature, ease and simplicity of reagents preparation and application, and absence or presence of artifacts. Experimental results obtained when using Fry, oxalic acid, Lichtenegger-Blöch, Murakami, modified Beraha, Kalling's Nº2, Ferrofluid 230300-135-3, and Ferrofluid EMG 911 reagents are presented in this paper. The advantages and drawbacks of these reagents in the study of the solidification modes in austenitic stainless steels under arc welding conditions are compared. As the conclusion of the current work, only Ferrofluid EMG 911 and Kalling's Nº2 reagents were found suitable based on the outlined criteria.

Introduction

In studying austenitic stainless steels, the microstructural characterization of the solidification modes (austenitic [A], austenitic-ferritic [AF], ferritic-austenitic [FA], and ferritic [F]) (Refs. 1–3) is of utmost importance. It is well known that the hot cracking phenomenon can be experienced by austenitic stainless steels while they are subject to certain heating/cooling processes and the temperature is around their melting point. This could happen during welding, casting, or hot forming. During the primary austenitic solidification modes (A, AF), the presence of impurities such as sulfur, phosphorus, and boron tend to segregate to the liquid phase and form low-melting point eutectics, which are distributed along the boundaries of dendrite grains at the last stages of solidification, causing cracking under the force of cooling contraction. However, if the material solidifies primarily as δ-ferrite (FA, F), the solid-state transformation experienced ($\delta \rightarrow \gamma$) will make the material less susceptible to hot cracking due to the higher solubility of the impurities in the δ phase as well as the better cracking resistance of δ/γ interfaces than δ/δ or γ/γ interfaces where the eutectic liquid enriched with impurities has better grain boundary wettability. Therefore, the microstructural characterization of the transition between AF and FA solidification modes in austenitic stainless steels is essential in order to establish the material susceptibility to hot cracking. Microscopy is also useful to detect brittle phases in those austenitic stainless steels subject to high temperature cycles and containing high levels of δ-ferrite, due to possible spinodal decomposition ($\delta \rightarrow \alpha + \alpha'$) or σ-phase formation.

Recently, the author (Refs. 4, 5) established the influence of the alloying level, in terms of total value of chromium equivalent plus nickel equivalent ($C_{req} + Ni_{eq}$), on the transition between AF and FA solidification modes in austenitic stainless steel weld metals. Traditionally, the transition between solidification modes was related to a critical Cr_{eq}/Ni_{eq} ratio. However, the new results obtained by the author demonstrated that the total alloying level was a key factor in the transition between AF and FA solidification modes. In order to work on the microstructural characterization of the austenitic steel samples effectively, and considering the wide composition range and number of reagents proposed in the literature (Refs. 6–9), it was necessary to select a reagent that was capable to provide the best etching results with the samples involved in the study. Consequently, the reagents selection was carried out prior to the main microstructural assessment. This paper presents the results obtained from the reagent selection process. The advantages and drawbacks of eight different reagents were illustrated when they were employed to etch austenitic stainless steel weld metal in order to establish the microstructural characterization of their solidification modes.

A common feature of suitable metallographic reagents is the formation of a selective film on the surface according to the phases that are found in the sample. In this research, the reagent was requested to be selective in front of δ-ferrite and γ-austenite phases so that these two different phases could be identified by microscopy. The necessity to evaluate eight different reagents to find the most suitable ones comes from the well-known resistance that stainless steels show to acids. The selectivity of the reagent could be achieved by different mechanisms, such as chemical or electrolytic etching, as well as magnetic fundamentals. Therefore, from the eight reagents considered here, five are based on chemical etching: Fry's reagent, Kalling's Nº2 reagent, Lichtenegger-Blöch's reagent, Beraha's reagent, and Murakami's reagent. The last three are considered color etchants (Ref. 9). The colors observed by optical microscopy de-

KEYWORDS

Metallographic Reagents
Ferrofluid
Austenitic Stainless Steels
Arc Welding

M. ASUNCIÓN VALIENTE BERMEJO (valiente.asun@gmail.com) is an independent researcher and consultant, Barcelona, Spain.

Fig. 1 — Transversal cross section.

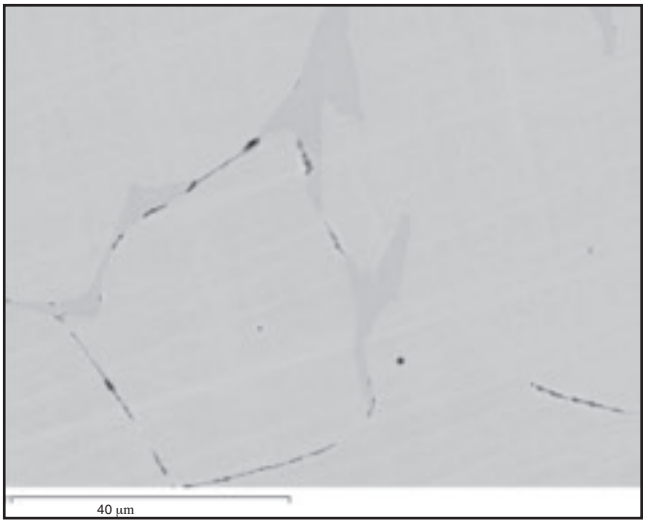

Fig. 2 — Faint contrast between austenite and ferrite. Fry's reagent.

pend on the thickness of the nonmetallic film formed as a result of the chemical reaction between the steel specimen and the reagent. These also depend on the etching conditions and crystallographic orientation of the particular phase. Other reagents used in this research are the oxalic acid, which acts through the electrolytic mechanism, and the ferrofluids, which achieve etching results based on the magnetic nature of the ferritic phase.

The magnetic response of δ-ferrite and the paramagnetism of γ-austenite is the basis for the magnetic etching technique. Initially, the technique was developed by Bitter in 1931 and consisted of sprinkling magnetic powder on the surface of a material under the effect of a magnetic field. Since then, the technique has advanced in order to improve the practical application (Ref. 10). Nowadays, the ferrofluids are colloids of iron (II, III) oxide nanoparticles (10 nm approximately) in a liquid solvent covered by a surfactant, which avoids particle agglomeration and stabilizes the suspension. The size and concentration of particles, type of surfactant, and solvent or liquid carrier are variables that promote a wide range of commercial ferrofluids of which the main industrial applications are related to audio speakers manufacturing and biomedical (Refs. 11, 12). Practically, ferrofluids are currently not commercially used as magnetic reagents, although some researchers (Refs. 10, 13, 14) have successfully used them to identify γ-austenite and δ-ferrite phases in duplex stainless steels since 1985. Ferrofluids have also been used as reagents in different applications such as revealing the magnetic domain structures of $Fe_{78}B_{13}Si_9$ metallic glass ribbons (Ref. 15), or contrasting austenite from martensite in dissimilar weld joints (Ref. 16).

Experimental Procedure

Two series of austenitic steel specimens were designed and prepared; the first one consisted of 45 samples with a constant alloying level of $Cr_{eq}+Ni_{eq}$ = 40 wt-% and the second one consisted of 42 samples with a constant alloying level of $Cr_{eq}+Ni_{eq}$ = 30 wt-%. While the alloying level was kept constant, the Cr_{eq}/Ni_{eq} ratio was gradually increased from 1.22 up to 2.00. Chromium and nickel equivalents (Cr_{eq}, Ni_{eq}) were calculated using the expressions established by Hammar and Svensson (Ref. 17). The base materials used for sample preparation were three grades of solid wires for gas tungsten arc welding (GTAW), including one mild steel grade (AWS A5.18 ER70S-6) and two austenitic grades (AWS A5.9 ER310 and ER312). The intended different alloying compositions were prepared using different weight combinations of these wires.

The precleaned wires were cut into segments between 10–18 mm in length and mixed in required proportions so that the designed different levels of $Cr_{eq}+Ni_{eq}$ and Cr_{eq}/Ni_{eq} ratios were achieved. The total weight of each batch of the samples was 50 g, which were melted in a pure argon atmosphere using the electric arc remelt furnace based on GTAW process recommended by the ASTM E1306-07 (Ref. 18).

The solid and homogeneous sample obtained was then cut into two halves by a cooled and lubricated alumina sawblade (Abrasive Cutter Buehler Metaserv). The transversal cross section of the cut surface (Fig. 1) was ground and polished according to standard metallographic preparation procedures. These included silicon carbide grinding papers P400, P600, and P1200 (Buehler-Met®) being sequentially used on a sloped wet manual device, and polishing was carried out on semiautomatic turntables (500 rev/min fixed rotational speed) using polishing cloths and diamond suspensions (Buehler MetaDi®) of 6 and 1 µm sizes. Polishing up to 0.25 µm diamond size was initially considered, and some samples were prepared. But it was dismissed as soon as it was proved that a too long polishing process was not further improving the surface, instead it introduced new undesired thinner scratches. It is well known how sensitive stainless steels are to surface deformation in metallographic preparation; therefore, it was necessary to find a compromised balance between doing the best possible final polish with the lowest diamond size and getting a totally deformation-free surface for microstructural characterization. It was also recognized that surface deformation could have been avoided in some events if the available semiautomatic turntables had worked at lower and variable rotating speeds, and also if the grinding process

Table 1 — Reagents and Their Chemical Compositions

Reagent	Chemical composition	Ref.
Fry's Reagent	5g $CuCl_2$ + 40 mL HCl (37%)+ 30 mL distilled H_2O + 25 mL absolute ethanol	6
Oxalic acid 10%	10 g oxalic acid + 90 mL distilled H_2O	6
Lichtenegger-Blöch	20 g NH_4HF_2 + 0.5 g $K_2S_2O_5$ +100 mL distilled H_2O	7, 20
Murakami's Reagent	10 g $K_3Fe(CN)_6$ + 10 g NaOH + 100 mL distilled H_2O	6, 8
Modified Beraha	2 g NH_4HF_2 + 1 g $K_2S_2O_5$ + 20 mL HCl (37%) + 80 mL distilled H_2O	9, 20
Kalling's N°2	5 g $CuCl_2$ + 100 mL HCl (37%) + 100 mL absolute ethanol	6, 8
Ferrofluid 230300-135-3	$CoFe_2O_4$ colloid in water solvent	
Ferrofluid EMG 911	Fe_3O_4 colloid in organic solvent	

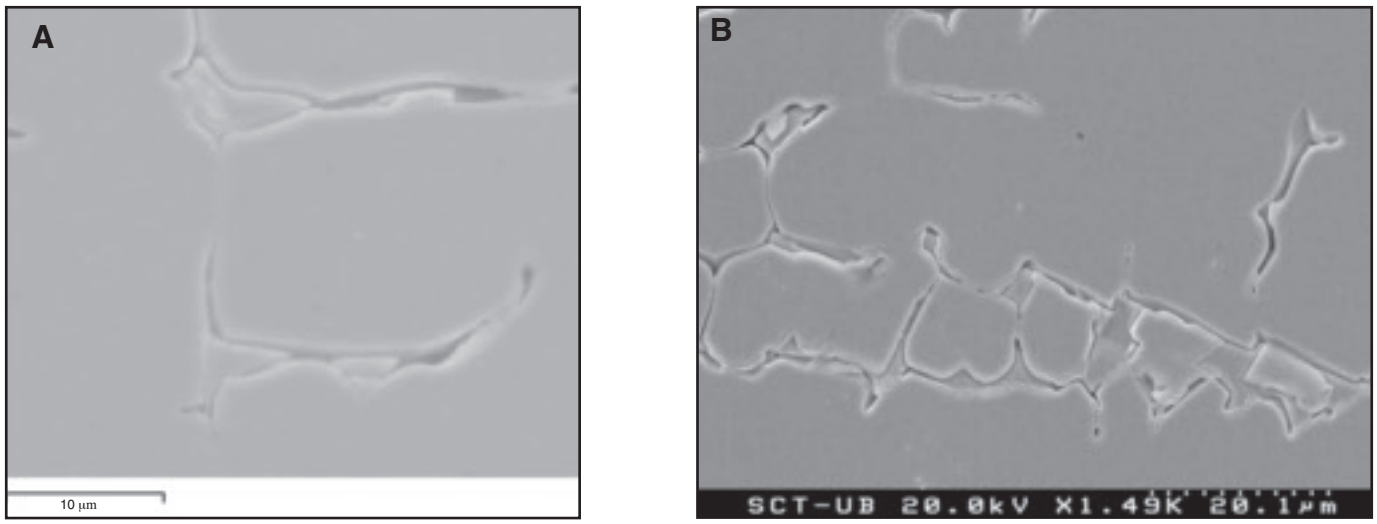

Fig. 3 — Oxalic acid etching on sample A31. A — SEM equipment; B — FEG-SEM equipment.

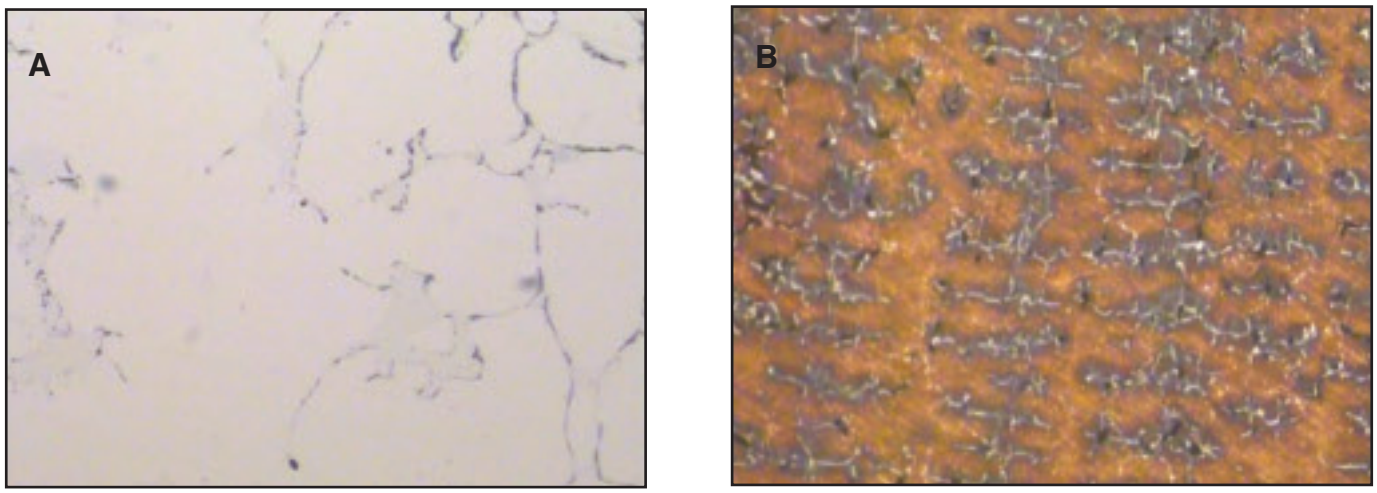

Fig. 4 — Lichtenegger-Blöch etching on sample A31. A — 30 s, hot (500x) ; B — 45 s at boiling (200x).

could have been done semiautomatically. The maximum time between the final polish and the etching was three days; meanwhile, samples were stored in a desiccator under vacuum condition.

The application of reagents was also conventional — applying the reagent on the surface of the specimen, leaving the reagent to etch for an established time, rinsing with distilled water, and drying the surface using ethanol and air. When using ferrofluids, there was a variation on the cleaning step, as it needed to be done with petroleum ether.

The chemical compositions of the eight reagents evaluated in this research are shown in Table 1. The reason for selecting these and not others was the availability in the laboratory of the primary components, together with the author's interest in exploring the effect of ferrofluids. Except for the ferrofluids, all reagents were prepared in situ by dissolving the primary components and were used immediately after preparation.

Optical microscopy (Axiovert 100A + Delta Pix Viewer LE Software) and scanning electron microscopy (SEM) equipped with energy dispersive X-ray spectroscopy (EDS) (Leica-Stereoscan 360) were used for microstructural characterization. Occasionally, for higher resolution, a field emission (FEG-SEM) equipment (Hitachi S-4100) was also used.

Results and Discussion

The transversal cross section of the designed stainless steel samples was etched using the eight proposed reagents listed in Table 1. In order to evaluate the suitability of each reagent, the following criteria were adopted: 1) absence of corrosion on the sample due to the reagent; 2) possibility of using conventional analysis equipment; 3) etching at room temperature; 4) good contrast between austenite and ferrite phases; 5) absence of artifacts or false visual effects; and 6) ease and simplicity to prepare and apply.

Details of the test conditions, advantages, and drawbacks found for each reagent are presented here. Based on the test results, those reagents considered as the optimum ones are introduced, and some micrographs of austenitic stainless steel solidification modes are also depicted together with the different δ-ferrite morphologies observed.

Fry's Reagent

The immersion time recommended by the bibliography (Ref. 6) ranged from a few seconds up to one minute. Initially the immersion time established was 10's, but an immediate pitting corrosion effect was observed. Therefore, in order to slow down the etching speed, some trials were carried out decreasing the immersion time and adding some extra ethanol from the initial quantity established in the literature (Table 1). Finally, the optimum etching condition was determined as 2 s with 20 mL of extra ethanol added, which made the final reagent composition to be 5 g $CuCl_2$, 40 mL HCl (37%), 30 mL distilled H_2O, and 45 mL absolute ethanol.

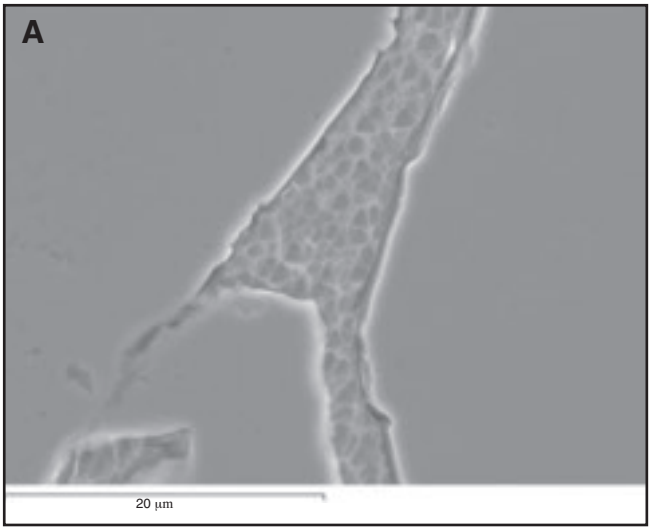

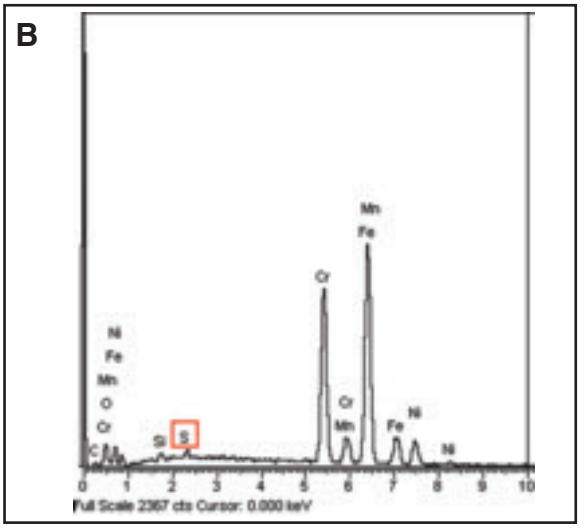

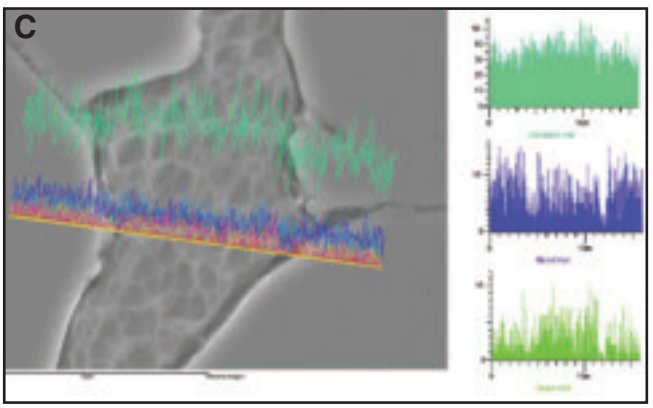

Fig. 5 — Beraha's etching on sample A31. A — Micrograph; B — spot microanalysis inside the δ-ferrite dendrite; C — linear microanalysis.

Using the optimized etching condition, 6 samples with different solidification modes were prepared for SEM microscopy assessment. However, observation showed that this reagent did not reveal the different microstructures properly, as it was not possible to distinguish austenite from ferrite clearly — Fig. 2. All attempts in varying the immersion time to increase the contrast between the phases resulted in the occurrence of pitting corrosion.

Based on the above results, Fry's reagent was rejected.

Electrolytic Etching Using Oxalic Acid (10%)

For electrolytic etching using oxalic acid (10%), the parameters recommended by the bibliography (Ref. 6) were 6 V from a few seconds up to one minute. In the current study, the equipment available only worked at a preset value of around 5 V, and it was not possible to determine the accurate value of the voltage or to change it. In order to find the optimal etching time, some trials were carried out at 15, 30, 40, and 60 s with two samples of different solidification modes but with a similar Cr_{eq}/Ni_{eq} ratio, samples A49 and A31. In the case of sample A49, $Cr_{eq}+Ni_{eq}$ was 30 wt-%, Cr_{eq}/Ni_{eq} ratio was 1.45 with a ferrite content of 0.89 FN, and its solidification mode was AF/FA. For sample A31, the solidification mode was FA, $Cr_{eq}+Ni_{eq}$ was 40 wt-%, Cr_{eq}/Ni_{eq} ratio was 1.44 and ferrite content 7.18 FN.

Results showed that 30 s of etching were sufficient for samples with FA solidification mode (Sample A31). However, neither optical microscopy nor the Leica SEM microscopy were able to provide acceptable images (Fig. 3A), and it was necessary to employ the Hitachi SEM equipment fitted with field emission — Fig. 3B. The advantage of this equipment was that the electron beam was thinner and this guaranteed a resolution up to 1.5 nm. But the downsides were that the equipment did not provide EDS microanalysis, and it also had limitations in accommodating the dimensions of the samples used in the current work.

On the other hand, the sample with mainly AF solidification mode (sample A49) remained unaffected after 60 s of etching, and it was not possible to observe any signs of etching on the ferrite phase by SEM microscopy.

Therefore, electrolytic etching using oxalic acid (10%) was rejected due to the low sensitivity shown for the samples with low ferrite contents (AF solidification mode), and the necessity of using a field emission equipment in order to have an acceptable image resolution for samples with higher ferrite contents (FA solidification mode). The impossibility to accurately control the voltage in the electrolytic cell was also taken into consideration.

Lichtenegger-Blöch Reagent

For some authors (Refs. 7, 19), the most interesting feature of this reagent was the fact that it could reveal the primary solidification microstructure experienced by the samples. The ferrite phase is usually dissolved by chemical etchants, and that is the reason why primary microstructure is not commonly revealed. However, despite having experienced the solid-state transformation $\delta \rightarrow \gamma$, if the sample is etched using Lichtenegger-Blöch's reagent at room temperature (Ref. 20), samples with FA solidification mode should show the primary ferrite dendrite core in white, the primary solidification microstructure in blue (austenite in case of AF or ferrite in case of FA), and the former interdendritic liquid in brown yellow.

After several trials using Beraha reagents, which are known by etching the ferrite phase based on the breakdown of the $K_2S_2O_5$ in a HCl medium, the researchers P. Lichtenegger and R. Blöch (Ref. 7) concluded that the replacement of the HCl used by Beraha for NH_4HF_2 used in the Lichtenegger-Blöch's reagent had the advantage to prevent the chromium-enriched ferrite (primary dendrite core) from being etched.

In the current work, sample A31 ($Cr_{eq}+Ni_{eq}$ = 40 wt-%, Cr_{eq}/Ni_{eq} = 1.44, FA, 7.18 FN) was subject to the reagent for 30 s both at room temperature and in hot conditions. Results showed that the sample was not etched at either conditions and the effect was faint — Fig. 4A. Etching time and temperature were then increased up to 45 s in boiling condition. Under this extreme condition, the reagent revealed the primary solidification mode (Fig. 4B), giving primary ferrite dendrite core in white, ferrite dendrite in blue, and inter-

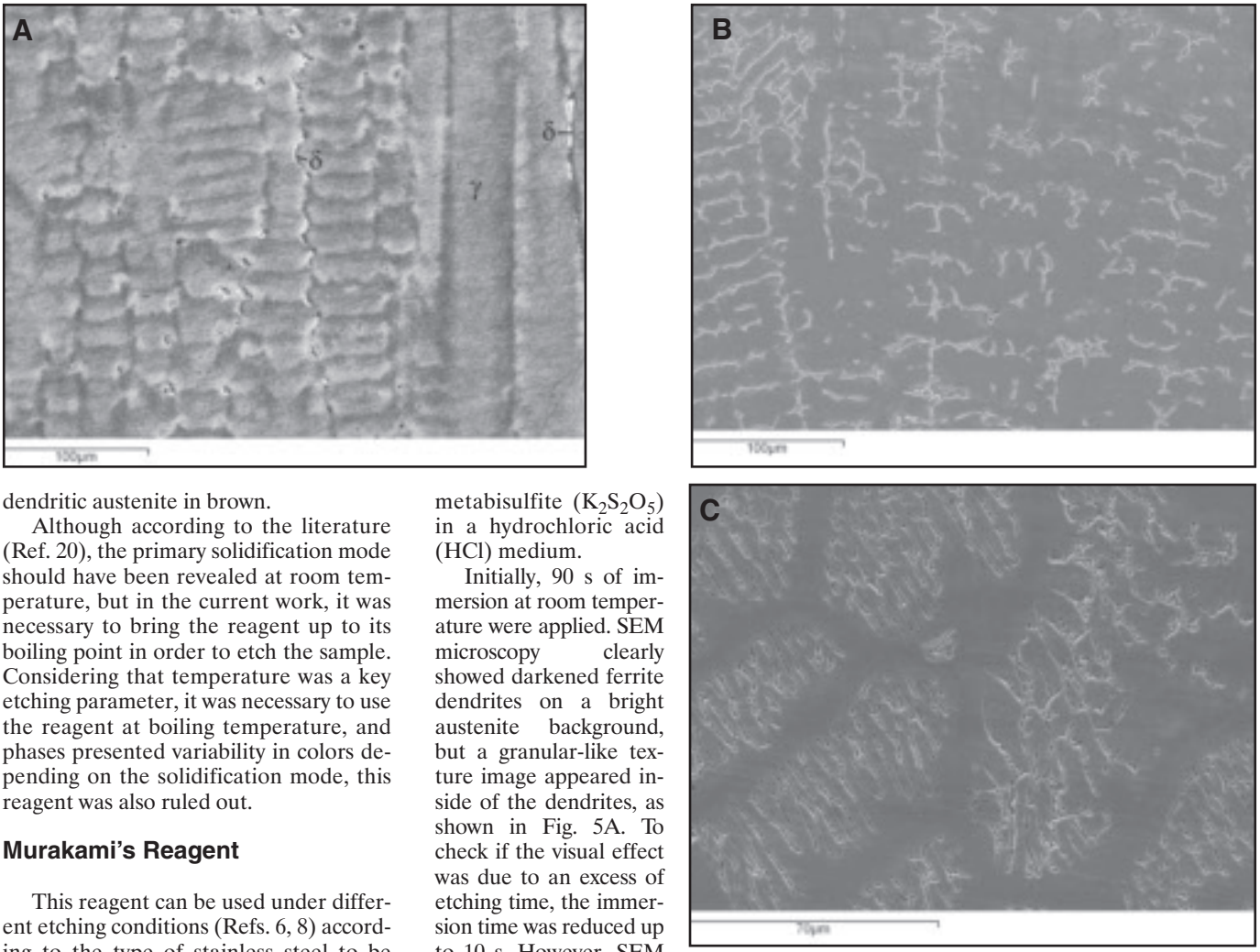

Fig. 6 — Kalling's No. 2 reagent. A — Eutectic ferrite in AF solidification mode; B — skeletal ferrite morphology in FA solidification mode; C — lathy ferrite morphology in FA solidification mode.

dendritic austenite in brown.

Although according to the literature (Ref. 20), the primary solidification mode should have been revealed at room temperature, but in the current work, it was necessary to bring the reagent up to its boiling point in order to etch the sample. Considering that temperature was a key etching parameter, it was necessary to use the reagent at boiling temperature, and phases presented variability in colors depending on the solidification mode, this reagent was also ruled out.

Murakami's Reagent

This reagent can be used under different etching conditions (Refs. 6, 8) according to the type of stainless steel to be analyzed. In the current study, it was used at room temperature for 5 and 10 s of immersion, although the literature suggested an interval of between 5 and 60 s.

According to Refs. 6 and 8, colors to be observed should be dark yellow for ferrite and white for unaffected austenite, or brown in case the etching time was too long.

However, keeping the sample immersed for the minimum etching time, a wide range of color shades was observed from the yellow, cinnamon, and brown under optical microscope. It was, therefore, not possible to clearly distinguish the phases due to the similarity in colors.

Possibly the main utility of this reagent would be with those samples of which the detection of sigma phase is crucial, as sigma phase in front of Murakami's reagent would show a bright blue color in contrast with the rest of yellow-brown phases.

Modified Beraha's Reagent

Beraha's reagents include a large number of different types (Refs. 7, 9, 20). In the case of the specific reagent for stainless steels, the etching mechanism is based on the production of sulfides from the aqueous solution of potassium metabisulfite ($K_2S_2O_5$) in a hydrochloric acid (HCl) medium.

Initially, 90 s of immersion at room temperature were applied. SEM microscopy clearly showed darkened ferrite dendrites on a bright austenite background, but a granular-like texture image appeared inside of the dendrites, as shown in Fig. 5A. To check if the visual effect was due to an excess of etching time, the immersion time was reduced up to 10 s. However, SEM microscopy continued showing the granular-like texture inside the ferrite dendrites. Therefore, the possibility of an excessive etching was ruled out.

An EDS spot microanalysis inside the dendrite (Fig. 5B) and a linear microanalysis (Fig. 5C) were carried out. Both results showed the presence of sulfur inside the ferritic dendrite, which was completely unusual according to the results obtained when the same sample was etched with other reagents. On the other hand, as it was already expected and explained by microsegregations during the solidification, the linear microanalysis confirmed the enrichment in chromium and depletion in nickel of the ferritic dendrite and the opposite trend in the austenitic matrix.

The origin and source of sulfur inside the ferritic dendrites could only be explained by the metabisulfite of the reagent. Therefore, considering that the granular morphology showed inside the dendrites was not observed with any of the other reagents, it was concluded that the modified Beraha's reagent very likely provoked a false visual effect or artefact. Consequently it was rejected.

Kalling's No. 2 Reagent

References 6 and 8 recommend immersion time of samples in Kalling's Nº2 reagent from a few seconds up a few minutes at room temperature. Different trials were conducted, and it was found that for samples with primary austenitic solidification mode, 2 s were suitable, but for primary ferritic samples between 8 to 10 s were necessary. Once the sample was etched, the ferrite phase was shown brighter and austenite matrix darker. It was proved that this reagent was able to resolve the inside of the ferritic dendrite and gave a good contrast between both phases without giving false artifacts. Therefore, it was considered as the main reagent for the microscopical study of the samples.

Good contrast between ferrite and austenite matrix is illustrated in Fig. 6A–C where the three main ferrite morphologies for austenitic stainless steels are depicted: eutectic (A), skeletal (B), and lathy (C).

This reagent was successfully used (Refs.

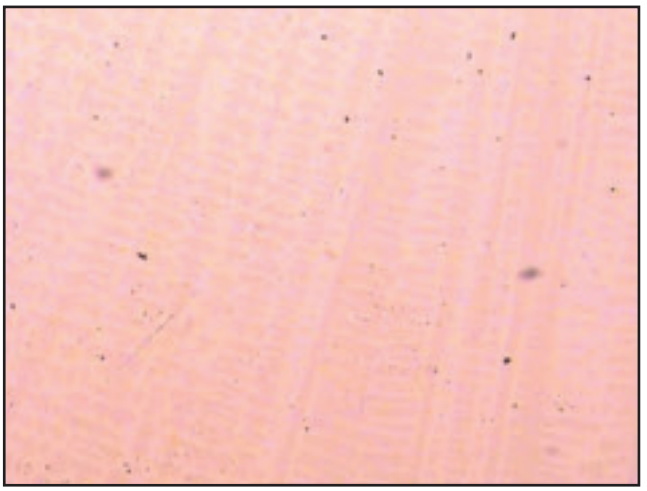

Fig. 7 — Ferrofluid 230300-135-3 on A, Sample A36. (500×).

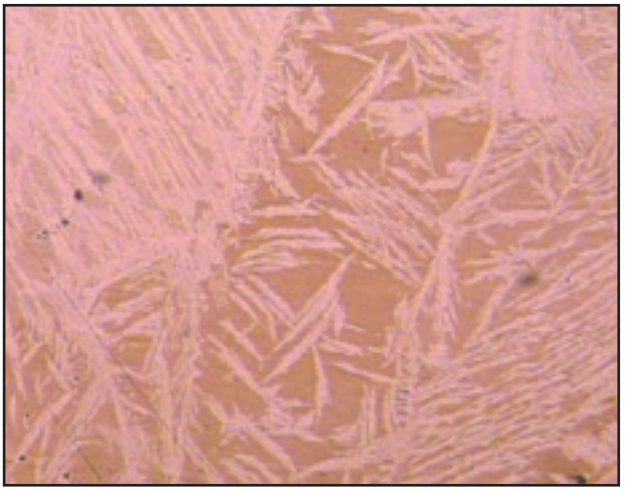

Fig. 8 — Ferrofluid 230300-135-3 on F, Sample A02. (500×).

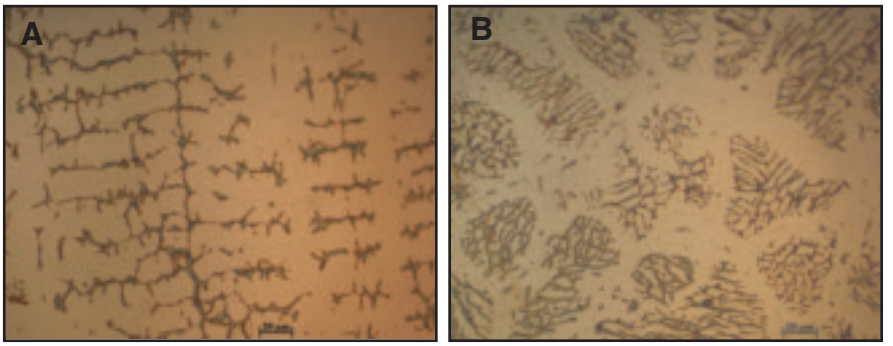

Fig. 9 — Ferrofluid EMG 911 on FA. A — Sample A32, skeletal ferrite morphology; B — Sample A57R, lathy ferrite morphology.

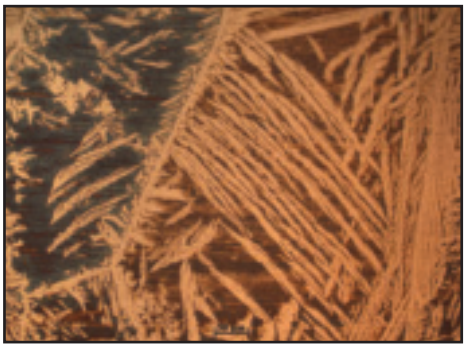

Fig. 10 — Ferrofluid EMG 911 on F, Sample A02.

4, 5) in order to establish the influence of the alloy level on the transition between AF and FA solidification modes in weld metals of austenitic stainless steels. Within a range of samples, it was possible to confirm the coexistence of eutectic ferrite at the interdendritic boundary of primary austenite dendrites with skeletal ferrite confirming primary ferritic solidification.

Ferrofluid 230300-135-3

Ferrofluid 230300-135-3 is a $CoFe_2O_4$ colloid in water solvent. In order to evaluate this reagent's behavior, it was applied to the transversal cross section of a completely austenitic sample, A36 (Cr_{eq}/Ni_{eq}= 1.22, [Cr_{eq}+Ni_{eq}] = 30 wt-%), and to a completely ferritic sample, A02 (Cr_{eq}/Ni_{eq}> 3).

According to the fundamentals of the technique, it would have been expected that the residual magnetism of the $CoFe_2O_4$ acted on the ferritic phase and would have not affected the austenite. However, as it is shown in Figs. 7 and 8, both phases, ferrite and austenite, experienced a chemical etch. It was thought that the chemical etch was due to the fact that a cation exchange resin with SO_3^{2-} groups was used during the ferrofluid's production, and its subsequent processing with water caused the final ferrofluid to contain protonated sulfites, which were responsible for the chemical etching on the samples, independently from the level of magnetism. Therefore, despite it could seem from the pictures that the reagent is able to contrast austenite phase from ferrite phase, the fact is that this ferrofluid is not able to contrast both phases by the expected residual magnetism mechanism.

Ferrofluid EMG 911

Ferrofluid reference EMG 911 is a colloidal suspension which contains 2 vol-% of Fe_3O_4 particles of 10 nm nominal size in a light hydrocarbon medium.

Walker and Ginn (Ref. 14) obtained good results in 1987 using a commercial ferrofluid, which is not currently in the market, with a 3.3 vol-% concentration that they diluted up to 1 vol-% using petroleum ether. For the present research, ferrofluid EMG 911 was diluted up to 1 vol-% Fe_3O_4 solution using the solvent EMG 900, which is an isoparaffinic hydrocarbon.

Samples with different solidification modes were selected: A01 (Cr_{eq}/Ni_{eq}<1.22) for A mode, A32 (Cr_{eq}/Ni_{eq} = 1.46) and A57R (Cr_{eq}/Ni_{eq} = 1.59) for FA mode, and A02 (Cr_{eq}/Ni_{eq}>3) and A731 (Cr_{eq}/Ni_{eq} = 2.00) for F mode.

Very satisfactory results were obtained, as none of the samples was chemically etched, and the austenite and ferrite phases were extremely contrasted colorfully using optical microscopy.

Once the ferrofluid is applied and the sample is then rinsed with petroleum ether, the austenite phase is free from the nanoparticles of iron oxide, and the strength of the residual magnetism between the nanoparticles and the ferritic phase makes the nanoparticles be deposited on the ferrite phase with different thickness layers. The higher chromium enriched ferrite provokes higher residual magnetism and, consequently, the higher thickness of Fe_3O_4 nanoparticles layers, and a darker color is observed using optical microscopy.

Figures 9 and 10 illustrate the colorful contrast between austenite phase in white and ferrite phase in blue or dark brown. Figure 9 depicts FA solidification mode with Fig. 9A showing the skeletal ferrite morphology, while Fig. 9B presents the lathy ferrite morphology. Figure 10 shows F solidification mode with characteristic Widmanstätten austenite plates.

Conclusions

Although the literature has introduced many reagents for metallographic etching of stainless steel welds, it has been found that a previous selection among reagents is necessary in order to ensure first, a good contrast between austenite and ferrite phases, and second, to confirm the absence of artifacts or corrosion due to the undesirable effect of reagent. It is also important that reagent preparation and application are simple and easy (better if etching can take place at room temperature), and that conventional microscopy equipment is able to provide good results.

Fry's reagent has not been selected because of the difficulties in setting a proper immersion time in order to get an acceptable contrast between the phases but without provoking pitting corrosion in the samples.

Oxalic acid was rejected due to the low sensitivity shown for ferrite phase, and the requirement for a field emission equipment in order to have an acceptable image resolution.

In the case of Lichtenegger-Blöch's reagent, in order to have the samples etched adequately, it was necessary to use it at boiling temperature. This fact, together with the variability in colors of the phases depending on the solidification mode, made the reagent to be ruled out.

Murakami's reagent presented a wide range of color shades from yellow, cinnamon, and brown under optical microscope. Therefore, it was not possible to clearly distinguish the phases due to the similarity in colors.

Modified Beraha's reagent showed a granular-like morphology coupled with traces of sulfur inside the ferritic dendrites, which can be explained by the metabisulfite of the reagent. Consequently, it was rejected.

From the eight reagents evaluated, only Kalling's Nº2 and ferrofluid EMG 911 accomplished the established criteria. For microanalysis and SEM microscopy, Kalling's Nº2 would be the most suitable reagent, while for optical microscopy, Ferrofluid EMG 911 would be the most convenient one due to the excellent contrast between phases and the ease of application.

It is necessary to emphasise that although the physical background of ferrofluids is the same, not all the ferrofluids are able to contrast austenite from ferrite phases. It is necessary to check that the surfactant and solvents used during the manufacture of the ferrofluid are not provoking a chemical etch on the sample, as Ferrofluid 230300-135-3 does.

Acknowledgments

The author gratefully acknowledges the support of Metrode Products Ltd., and is specially indebted to Zhuyao Zhang and Adam W. Marshall for providing the welding consumables and facilities to carry out this research. The author also acknowledges Anna Julià from the University of Barcelona and Vanessa Rene from Ferrotec for the supply of ferrofluid reagents. The current research is part of the doctoral degree thesis entitled "Modelització del nivell de ferrita δ als acers inoxidables austenítics sotmesos a fusió per arc electric," which was submitted for the degree of doctor in chemistry by the author at the University of Barcelona the 29th of June, 2010. It is also gratefully acknowledged the supervision of Pere Molera and Núria Llorca from the Department of Materials Science and Metallurgical Engineering at the University of Barcelona.

References

1. Kujanpää, V. P., Suutala, N., Takalo, T., and Moisio, T. 1979. Correlation between solidification cracking and microstructure in austenitic and austenitic-ferritic stainless steel welds. *Welding Research International* 9(2): 55–75.

2. Kujanpää, V. P., Suutala, N., Takalo, T., and Moisio, T. 1980. Solidification cracking — estimation of the susceptibility of austenitic and austenitic-ferritic stainless steel welds. *Metal Construction* 12(6): 282–285.

3. Suutala, N. 1983. Effect of solidification conditions on the solidification mode in austenitic stainless steels. *Metallurgical Transactions A*. 14A(2): 191–197.

4. Valiente Bermejo, M. A. 2010. Modelització del nivell de ferrita δ (FN) als acers inoxidables austenítics sotmesos a fusió per arc electric. PhD dissertation. University of Barcelona. ISBN 978-84-693-5713-2.

5. Valiente Bermejo, M. A. 2011. IIW Document IX-2359-11 Influence of the alloy level [Cr_{eq}+Ni_{eq}] on the transition between AF and FA solidification modes in austenitic stainless steel weld metals. *64th Annual Assembly of the International Institute of Welding.* July, Chennai, India.

6. *ASM Metals Handbook*. 1973. Metallography, structures and phase diagrams. Vol. 8. 8th edition, pp. 97–99. ASM International. Ohio. ISBN 27-12046.

7. Lichtenegger, P., and Blöch, R. 1975. *Colour Etching of High Alloy Steels. Praktische Metallographie* 12: 567–573.

8. Lippold, J. C., and Kotecki, D. J. 2005. *Welding Metallurgy and Weldability of Stainless Steels*. New Jersey: Wiley-Interscience. ISBN 0-471-47379-0.

9. Vander Voort, G. F. 2005. Color metallography. *Microscopy Today* 13(6): 22–27. The Microscopy Society of America. ISSN 1551-9295.

10. Gray, R. J. 1986. Magnetic Etching. In Vander Voort, G. F. *Applied Metallography.* New York: Van Nostrand Reinhold Co., Chapter 4, pp. 53–61.

11. Raj, K., and Moskowitz, R. 1990. Commercial applications of ferrofluids. *Journal of Magnetism and Magnetic Materials* 85: 233–245.

12. Raj, K., Moskowitz, B., and Tsuda, S. 2004. New commercial trends of nanostructured ferrofluids. *Indian Journal of Engineering & Materials Sciences* 11: 241–252.

13. Ginn, B. J. 1985. A technique for determining austenite to ferrite ratios in welded duplex stainless steels. *The Welding Institute Research Bulletin*. November, pp. 365–367.

14. Walker, R. A., and Ginn, B. J. 1987. A magnetic "etching" technique for phase identification in duplex ferritic-austenitic and other stainless steels. *ASM Int. 19th Annual Technical Meeting. Field Metallography, Failure Analysis and Metallography.* Ohio: M. E. Blume, ed., vol. 15, pp. 519–528.

15. Birol, Y. 1998. Magnetic domain structures in as-quenched and annealed $Fe_{78}B_{13}Si_9$ metallic glass ribbons. *Turkish Journal of Physics* 22: 481–488.

16. Rowe, M. D., Nelson, T. W., and Lippold, J. C. 1999. Hydrogen-induced cracking along the fusion boundary of dissimilar metal welds. *Welding Journal* 78(2): 31-s to 37-s.

17. Hammar, Ö., and Svensson, U. 1979. Influence of steel composition on segregation and microstructure during solidification of austenitic stainless steels. *The Metals Society. International Conference on Solidification and Casting of Metals.* Sheffield (UK), pp. 401–410.

18. ASTM E1306-07. 2007. *Standard Practice for Preparation of Metal and Alloy Samples by Electric Arc Remelting for the Determination of Chemical Composition.* Philadelphia: ASTM International.

19. Folkhard, E. 1988. *Welding Metallurgy of Stainless Steels*. Vienna: Springer-Verlag. ISBN 3-211-82043-4.

20. Weck, E., and Leistner, E. 1983. *Metallographic Instructions for Colour Etching by Immersion. Part II: Beraha Colour Echants and their Different Variants*. Vol. 77/II. Düsseldorf: D.V.S. Verlag GmbH.